UDC 551.24

A. I. MANEVICH[1], *Researcher, Post-Graduate Student of the College of Mining, NUST MISIS*
V. N. TATARINOV[1], *Head of Laboratory, Doctor of Engineering Sciences, v.tatrinov@gcras.ru*
K. S. KOLIKOV[2], *Head of Chair, Doctor of Engineering Sciences*

[1] *Geophysical Center, Russian Academy of Sciences, Moscow, Russia*
[2] *College of Mining, National University of Science and Technology—MISIS, Moscow, Russia*

DETECTION OF CRUSTAL DEFORMATION ANOMALIES WITH REGARD TO SPATIAL SCALE EFFECT

The current standard criteria for horizontal strains at locations of nuclear power objects are set without regard to distances and observation times. Accordingly, the reference hazardous strain can either be overestimated or underestimated in a test scale of a region. This deteriorates reliability of the engineering safety criteria for satellite observation data on horizontal crustal movements. At the same time, the current legislation recommends taking into account spatial scaling when assessing deformation and velocities of recent crustal movements, though no specific practical guidance is provided. In this connection, this article presents the analysis results for observations over recent crustal movements on a few tens of geodynamic test grounds in the world.

The analysis procedure uses the algorithm for discrimination of stain classes, dilation and strain rates with regard to spatial scale effect. The algorithm is based on pattern recognition and enables predicting classes of strain hazard depending on distance or area to which the displacement is normalized. The article presents the analysis procedure and the results of the case-study for a geodynamic test ground located in a tectonically active region of the world.

Keywords: *geodynamics, strains, recent crustal movements, GPS, GLONASS, scale effect, pattern recognition.*
DOI: *10.17580/em.2019.02.04*

Introduction

In site selection and construction of ecologically hazardous objects, including nuclear power objects (NPO), a specific concern is justification of long-term geodynamic safety in this area. The geodynamically hazardous zones are widely revealed by surveying with Global Positioning Systems/Global Navigation Satellite Systems GPS/GNSS. Recent crustal movements (RCM) are measured on local geodynamic testing grounds (GDTG). Yet long before GPS, it was known that movements recorded on ground surface were *interference* of impacts from various scale and lifetime endogenous and exogenous geodynamic sources. The crustal blocks in the linear field of such sources carry out differently directed and alternate movements, which cumulatively result in a phenomenon of reduction in strain rates with distance between observation points. This critical property of a hierarchically structured geological medium is proved by M. A. Sadovsky, V. F. Pisarenko, S. I. Sherman, G. G. Kocharyan, Yu. O. Kuzmin and others [1–4].

Efficiency of GPS observations with baselines of thousand kilometers and longer formed an illusion on suitability of the method to engineering problems handled on local geodynamic testing grounds which are seldom more than 10 km in size. The methodology of GPS observation data interpretation was commonly extended from global to local scales. Some researchers used a block structure model of the Earth's crust (discrete medium) [5], while the others rely upon a continuum model [6]. At the same time, the interpretation of GNSS observation data faces a "fault–block" dilemma [4]: the dynamic element responsible for anomalous deformation is either the structural block or the block interface (fault) and the block is then a passive element. This results in difficulties in construction of GDTG networks and in engineering evaluation of GNSS observation results.

It is worthy of mentioning that it is critical for NPO that the safety criteria of engineering evaluation are reliable as the error of horizontal deformation may cost very much. For example, on the Crimea Nuclear Power Plant site, recent crustal movements have gradients of $8\cdot10^{-6}$ year^{-1} while the allowable inclination of critical structures is $3\cdot10^{-6}$ year^{-1} [7].

Objectives of the research

The current problem is that the available criteria for horizontal strains are set without regard to distances and times of observations on GDTG. For instance, Rostekhnadzor [8] defines an active fault as "a fault with recent movement velocity higher than 5 mm/yr." Apparently, in case of faults a few kilometers or a few hundred kilometers long, strains calculated by this criterion will differ by orders of magnitude. The new version of the document [9] recommends taking into account spatial scaling when evaluating deformation and RCM velocities.

The yearly mean strain rates in the areas of increased geodynamic hazard are presented in [4, 10]. The hazardous horizontal strain rate is D^3 $5\cdot10^{-4}$–10^{-5} per year. V. I. Ulomov [11] gives the strain rates for the Kazakhstan Shield and dynamic areas of Tian Shan as $5\cdot10^{-8}$ and 10^{-7} per year, respectively. The factor of time is also taken into account, for instance, in [10], by introduction an empirical coefficient to reflect the cyclic nature of recent crustal movements. The hazardous zone criterion is given by:

$$\theta > Ce_i/t, \tag{1}$$

where e_i are the calculated strains; C is the empirical coefficient ranging as 3–5 from the data of long-term repeated surveys; t is the time.

One of the first publications to generalize data of GNSS observations on different scales was the research by T. V. Guseva et al. [12]. The authors for the first time related moduli of strain rates and scales of distances based on the long-term monitoring results.

Obviously, strain rates in different publications scatter by orders of magnitudes depending on spacing of observation points. Accordingly, the objectives of the research were formulated as:

- creation of GNSS data catalogs for different tectonic areas and spatial scales of GDTG;
- spatial variability analysis and classing of strains, plotting of maximal and average strain rates for different scales and regions of different geodynamic behavior;
- verification of strain rate prediction at local GDTG, including locations of NPO, using the mentioned plots.

Below in this article, the results of the first two objectives aimed to develop unified engineering criteria for interpretation of strain rates on different scales in the earth crust are presented.

Data catalog of recent crustal movements

The data catalog of recent crustal movements has been collected from open-access electronic and analog sources. The cataloging specified that:

- GDTG had different scales, from units to thousands kilometers;
- GDTG located in the regions with different tectonic activity, from intraplatform areas to seismically hazardous zones on the Pacific shore.

The **table** lists the most popular electronic databases of GNSS observations involved in the cataloging. Currently, the catalog contains information on 92 geodynamic test grounds.

Classification of strain rates

Numerical series of strain rates are divided into two groups: the first group is strains of the background (quiescent) geodynamic behavior of the lithosphere; the second group is anomalous strains. The difficulty of grouping consists in the absence of discrimination criteria. In this study, the number of classes is only set, but the a priori information on belonging of a strain sampling element to a specific class is absent. The discrimination algorithm was developed. The algorithm description and the results of its testing in terms of the time series of observations carried out in California, USA, are given below.

The classification problem is generally formulated as follows. Let *X* be a set of strain rate calculations by GNSS data; it can be split into a set of classes $Y_1, \ldots, Y_i$. The integral division is unknown, and each class is short of subsets of elements with the known class belonging but the number of the wanted classes is assigned. Accordingly, the learning sampling is absent, and discrimination should be done using the “teacher-free” methods. Each element in the set possesses an attribute description $x = [f_1(x), \ldots, f_1(x)]$. It is required to build an algorithm to image the relationship *XY* capable to classify an arbitrary object $x \in X$.

The calculation can use different values characterizing RCM: dilation, linear or area deformation, etc. As a test parameter of spatial features of the horizontal RCM velocities, this study selects the rate of relative change in the distance (distance between two points on the surface of sphere) between GNSS observation points:

GNSS observation databases on RCM

No.	Database	Source
1	United States Geological Survey, GPS data	[13, 14]
2	The MAGNET GPS Network	[15]
3	Rete Integrata Nazionale GPS	[16]
4	GeoDAF. Geodetic Data Archiving Facility	[17]
5	Friuli Regional Deformation Network Data Center	[18]
6	EUREF Permanent GNSS Network	[19, 20]
7	GNSS Time Series	[21]
8	GNSS database UNAVCO	[22]
9	Scripps Orbit and Permanent Array Center (SOPAC)	[23]

$$\varepsilon' = \varepsilon/T, \quad (2)$$

where $\varepsilon = \Delta L/L$ is the relative change in the length *L* of the distance between two observation points in the time interval *T*.

The arc distance *L* (km) is found from the formula:

$$L = \arccos[\sin(\alpha_1) \cdot \sin(\alpha_2) + \cos(\alpha_1) \cdot \cos(\alpha_2) \cdot \cos(\beta_1 - \beta_2)] \times R, \quad (3)$$

where α_1, α_2 are the latitudes of the points; β_1, β_2 are the longitudes of the points; *R* is the average radius of the earth, it is assumed as 6371 km.

The diagram $\varepsilon'(L)$ is plotted based on the velocities of change in the distance between the observation points (mm/yr) normalized to their length. Then, the sequences of $\varepsilon'(L)$ are processed. Obviously, with increasing distance at uniform distributions of the absolute values of RCM, the strain $\varepsilon'(L)$ will decrease. This dependence will be replicated in case of any test ground with the change of the absolute coordinate position or angle of gradient.

An illustration of visualized data for two GDTG of different dimensions by an order of magnitude and located in the regions with different tectonic activity is shown in **Fig. 1**. The obtained data are the source for the discrimination. The database comprises the values of such attributes as:

- estimated strain rate;
- normalizing (distance, area, etc.);
- deviation $d\varepsilon'$ calculated from formula (5):

$$d\varepsilon' = \varepsilon'_i - \varepsilon'_{i+1}, \quad (5)$$

where *i* is a sequential number of the stain value;

- deviation *dL* given by:

$$dL = L - L_{i+1}. \quad (6)$$

- deviation density ψ:

$$\psi_i = \varepsilon'_i/L_i, \quad (7)$$

It is obligatory to calculate the deviation $d\varepsilon'$ with regard to the operator’s sign for the further discrimination to be feasible. As seen, the attribute space is synthesized from the values of the number series while the tectonic conditions of GDTG are ignored.

In this study, two classes of strains are distinguished: the values typical (conventionally “non-hazardous”) for the deformation behavior of GDTG; the values off the first group with higher absolute values (anomalous). Theoretically, the group of the anomalous strains can be both at the bottom and at the top of the diagram. This study is interested in the subset of strains hazardous for NPO; for this reason, the group *at the top of the diagram* is only chosen and the decision rules of prediction are formulated on this basis.

The decision rules are based on the analysis of excess over the deviation density ψ and estimated strain $\varepsilon'(L)$ by the threshold heuristic value $t_{\psi,\varepsilon}$:

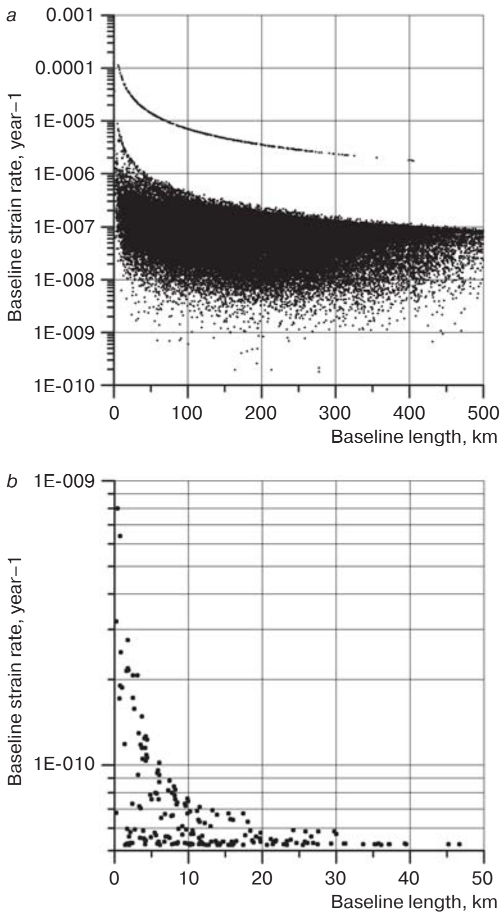

Fig. 1. Log chart ε′(*L*):
a — more than 90 000 baselines, test ground *Southern California Network* of USGS service [24]; *b* — 190 baselines, test ground in the Lower Kan Massif, Krasnoyarsk Territory [3].

$$\begin{cases} \varepsilon_i'(L) > t_s(i-n,\ i+n); \\ \begin{cases} \varepsilon_i'(L) > t_s(i-n,\ i+n); \\ \psi_i > t_\psi(i-n,\ i+n) \end{cases} \end{cases} \quad (8)$$

or in terms of the Boolean operators:

$$\varepsilon_i'(L) > t_s(i-n, i+n) \wedge (\varepsilon_i'(L) > t_s(i-n, i+n) \wedge \psi_i > t_\psi (i-n, i+n)), \quad (9)$$

where t is the threshold heuristic value of strain or deviation density in the neighborhood of values $i - n$, $i + n$; n is the half-interval for estimate of the threshold t.

The threshold t is calculated as the evaluation of the interval (window) of a chosen point in the neighborhood ($i - n, i + n$). The size of the interval is governed by the number of observation points (i. e. number of baselines) and their average frequency within the selected distance.

In this manner:

• *Rule* 1: $\psi_i > t_\psi$ — selecting offtype strains in the geodynamic behavior of a test GDTG;

• *Rule* 2: $\varepsilon_i'(L) > t_s$ — selecting anomalous excess strains;

• *Rule 3*: conjunction of Rules 1 and 2 — selecting anomalously high strains no typical of the geodynamic behavior of GDTG;

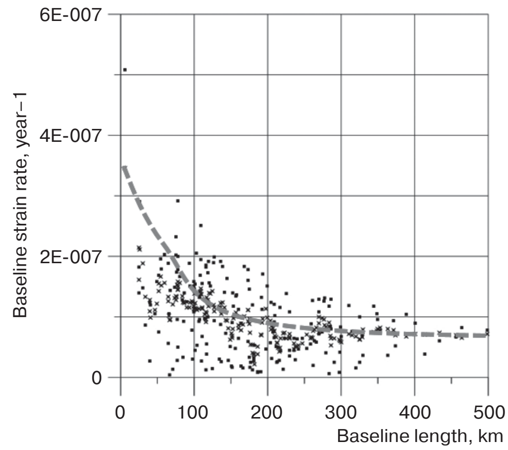

Fig. 2. Log chart ε′(*L*) by data from [24]:
1 — calculated values of arc length change rate ε′;
2 — averaged strains over interval *2n* = 7

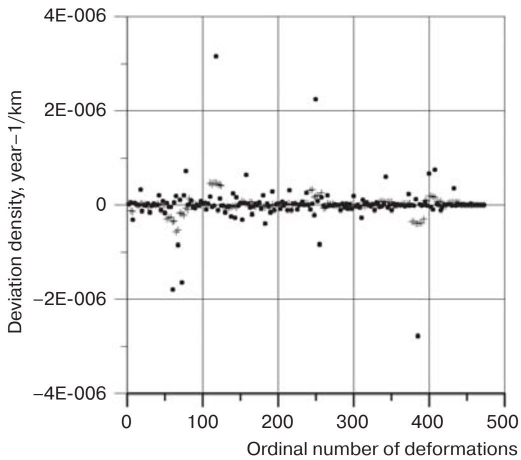

Fig. 3. Diagram of deviation density ψ:
1 — calculated values of deviation density ψ;
2 — averaged deviation densities over interval *2n* = 7

• *Rule 4*: conjunction of Rules 2 and 3 — selecting intersections of anomalously high strains and anomalously high strains not typical of the geodynamic behavior of GDTG.

This procedure uses simple estimates for selecting strain anomalies. The threshold t is selected empirically or by experts. The procedure enables correction and adaptation to more specific objectives of strain grouping.

Analytical results

Below, a case-study of calculations performed for a test sampling of data on the test ground Southern California Network of USGS service is presented [24].

We calculate the rate of relative change in the distance between geodetic points from (6) and obtained a cloud of points to be analyzed. This cloud and the series of of strain averaged over the interval of seven values are shown for the demonstrativeness in **Fig. 2**. The values of the deviation density ψ are presented in **Fig. 3** also alongside with the averaging over the interval of seven values.

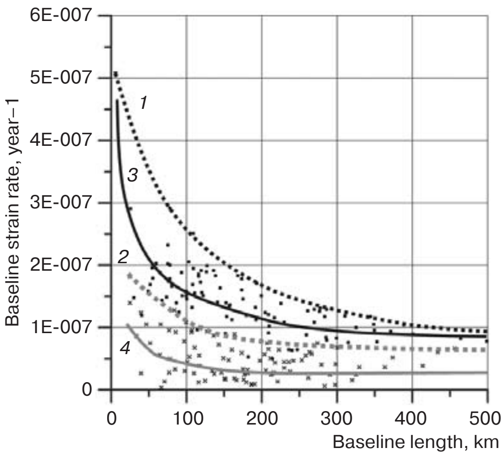

Fig. 4. Diagram of distinguished strain rates on the test ground:
1 — upper boundary of anomalous strain rates; 2 — boundary between strain rate classes; 3 — average values in the group of anomalously high strain rates; 4 — average values in the group of background strain rates
Squares — high strain rates; criss-crosses — typical strain rates (group 1)

Application of the algorithm of decision rules to the test data sampling allows identifying two classes of strains. The calculation results are shown in **Fig. 4**. It is worth mentioning that this example is unsuitable for the analysis of the compression–tension strains as the arc length formula (2) is not intended for that. However, it is possible to plot individual diagrams for any type strains and analyze them.

These results allow two classes to be distinguished in the data cloud—strain rates typical of the geodynamic behavior in the test region, which are assumed as non-hazardous, and higher strain rates assumed as hazardous. The hazardous strains are determined for each distance to which ground surface displacement recorded by GNSS is normalized. The obtained results are applicable in development of new engineering criteria of NPO operation safety with regard to the scale effect, or in assessment of geodynamic behavior in the test ground. Thus, the algorithms of processing, including neural nets [25] of data on RCM velocities using GNSS observations can enable highly reliable detection of areas with anomalously high strain rates on ground surface.

Acknowledgments

This work was conducted in the framework of the state contract concluded with the Geophysical Service of the Russian Academy of Sciences and approved by the Ministry of Education and Science of the Russian Federation.

References

1. Sadovsky M.A., Pisarenko V. F. Seismic process in a blocky medium. Moscow : Nauka, 1991. 96 p.
2. Kocharyan G. G. Scale effect in seismotectonics. *Geodynamics & Tectonophysics*. 2014. Vol. 5(2). pp. 353–385.
3. Sherman S. I., Bornyakov S. A., Buddo V. Yu. Dynamic impact zones of faults. Novosibirsk : Nauka, 1983. 112 p.
4. Kuzmin Yu. O. Recent geodynamics of fault zones : faulting in a real-time scale. *Geodynamics & Tectonophysics*. 2014. Vol. 5, No. 2. pp. 401–443.
5. McCaffrey R. Block kinematics of the Pacific–North America plate boundary in the Southwestern United States from inversion of GPS, seismological, and geologic data. *Journal of Geophysical Research*. 2005. Vol. 110. B07401. DOI:10.1029/2004JB003307.
6. Meade B. Present-day kinematics at the India–Asia collision zone. *Geology*. 2007. Vol. 35. pp. 81–84.
7. Tatarinov V. N., Tatarinova T. A. Inclusion of scale effect in satellite observations over ground surface deformation. *Marksheiderskii vestnik*. 2012. No. 5. pp. 15–19.
8. Safety Code RB-019-01. Seismic hazard estimation at locations of nuclear power and radiation objects by geodynamic data. Moscow, 2011.
9. Safety Code RB-019-17. Initial seismicity estimation in a region and site of nuclear objects during engineering survey and investigations. Moscow, 2018.
10. Kuzmin Yu. O. Recent geodynamics of dangerous faults. *Izvestiya. Physics of the Solid Earth.* 2016. No. 5. pp. 709–722.
11. Ulomov V. I. Role of horizontal tectonic movements in seismogeodynamics and seismic hazard prediction. *Fizika Zemli.* 2004. No. 9. pp. 14–30.
12. Guseva T. V., Mishin A. V., Skovorodkin Yu. P. Present-day movements in different scales. *Fizika Zemli*. 1996. No. 12. pp. 86–91.
13. GPS data. USGS Earthquake Hazards Program. Available at: https://earthquake.usgs.gov/monitoring/gps (accessed: 01.03.2019).
14. Murray J. R. Svarc J. Global positioning system data collection, processing, and analysis conducted by the U.S. Geological Survey Earthquake Hazards Program. *Seismological Research Letters*. 2017. Vol. 88. pp. 916–925.
15. MAGNET GPS Network. Nevada Geodetic Laboratory. Available at: http://geodesy.unr.edu/magnet.php (accessed: 01.03.2019).
16. Data Repository. Rete Integrata Nazionale GPS. Available at: http://gsac.gm.ingv.it:8080/prototypegsac (accessed: 01.03.2019).
17. GPS: Data & Products. Geodetic Data Archiving Facility. Available at: http://geodaf.mt.asi.it/gps_data_solutions.html (accessed: 01.03.2019).
18. FReDNet DC, Friuli Regional Deformation Network Data Center. Istituto Nazionale di Oceanografia e Geofisica Sperimentale. Dataset 2016.
19. Bruyninx C., Habrich H., Söhne W., Kenyeres A., Stangl G., Völksen C., Enhancement of the EUREF permanent network services and products. *Geodesy for Planet Earth. IAG Symposia Series*. 2012. Vol. 136. pp. 27–35.
20. EUREF permanent GNSS network. Available at: http://www.epncb.oma.be/ (accessed: 01.03.2019).
21. GNSS time series. NASA. https://sideshow.jpl.nasa.gov/post/series.html (accessed: 01.03.2019).
22. UNAVCO Data Center. Available at: https://www.unavco.org/ (accessed: 01.03.2019).
23. Scripps Orbit and Permanent Array Center (SOPAC). Available at: http://sopac-csrc.ucsd.edu/index.php/sopac/ (accessed: 01.03.2019).
24. GPS Data (USGS Earthquake Hazards Program). Available at: https://earthquake.usgs.gov/monitoring/gps/Southern_California/velocities (accessed: 01.03.2019).
25. Tatarinov V. N., Manevich A. I., Losev I. V. System approach to geodynamic zoning based on artificial neural networks. *Gornye nauki i tekhnologii.* 2018. No. 3. pp. 14–25. DOI: 10.17073/2500-2018-14-25.